Bioorganic & Medicinal Chemistry Letters xxx (2016) xxx–xxx

Contents lists available at ScienceDirect

Bioorganic & Medicinal Chemistry Letters

journal homepage: www.elsevier.com/locate/bmcl

Synthesis and evaluation of a series of 4-azaindole-containing p21-activated kinase-1 inhibitors

Wendy Lee [a,*], James J. Crawford [a], Ignacio Aliagas [a], Lesley J. Murray [b], Suzanne Tay [b], Weiru Wang [c], Christopher E. Heise [d], Klaus P. Hoeflich [e,†], Hank La [b], Simon Mathieu [a,‡], Robert Mintzer [d], Sreemathy Ramaswamy [d], Lionel Rouge [c], Joachim Rudolph [a]

[a] Discovery Chemistry, Genentech, Inc., 1 DNA Way, South San Francisco, CA 94080, USA
[b] Drug Metabolism and Pharmacokinetics, Genentech, Inc., 1 DNA Way, South San Francisco, CA 94080, USA
[c] Structural Biology, Genentech, Inc., 1 DNA Way, South San Francisco, CA 94080, USA
[d] Biochemical and Cellular Pharmacology, Genentech, Inc., 1 DNA Way, South San Francisco, CA 94080, USA
[e] Translational Oncology, Genentech, Inc., 1 DNA Way, South San Francisco, CA 94080, USA

ARTICLE INFO

Article history:
Received 13 May 2016
Revised 10 June 2016
Accepted 11 June 2016
Available online xxxx

Keywords:
PAK1
Kinase
4-Azaindole
Aminopyrazole
Diaminopyrimidine

ABSTRACT

A series of 4-azaindole-containing p21-activated kinase-1 (PAK1) inhibitors was prepared with the goal of improving physicochemical properties relative to an indole starting point. Indole **1** represented an attractive, non-basic scaffold with good PAK1 affinity and cellular potency but was compromised by high lipophilicity ($c\log D = 4.4$). Azaindole **5** was designed as an indole surrogate with the goal of lowering $\log D$ and resulted in equipotent PAK1 inhibition with a 2-fold improvement in cellular potency over **1**. Structure–activity relationship studies around **5** identified additional 4-azaindole analogs with superior PAK1 biochemical activity (K_i <10 nM) and up to 24-fold selectivity for group I over group II PAKs. Compounds from this series showed enhanced permeability, improved aqueous solubility, and lower plasma protein binding over indole **1**. The improvement in physicochemical properties translated to a 20-fold decrease in unbound clearance in mouse PK studies for azaindole **5** relative to indole **1**.

The p21-activated kinases (PAKs) are serine-threonine protein kinases in the sterile-20 (STE20) family and play significant roles in cytoskeletal rearrangement, cellular morphogenesis, and survival.[1] There are six isoforms in the PAK family, divided into two subfamilies based on sequence homology: PAK1–3 (group I) and PAK4–6 (group II). Group 1 PAKs are activated by Cdc42 or Rac1 interaction with GTPase-binding that overlaps with an auto-inhibitory domain.[1,2] The mechanism of activation of group II PAKs is less clear, and its prominent difference from group I PAKs is the lack of Rho GTPase-mediated activation.[2,3] The most studied isoform is PAK1, and its involvement in tumorigenesis and metastasis is well validated and reviewed.[1,4,5] PAK1 has emerged as an attractive target for anticancer therapy and has become the subject of significant drug discovery efforts in the past few years.[6,7] PAK1 signaling is often upregulated in human tumors and PAK1 gene expression is elevated in various human cancers, including subsets of breast, ovarian, and colorectal carcinoma. In recent years there have been several studies suggesting therapeutic potential of small molecule PAK1 inhibitors in breast cancer cell lines[8] and in ovarian cancers that are characterized by PAK1 gene amplification.[9] To date, no PAK inhibitor has advanced to proof-of-concept studies in human. A PAK1 selective inhibitor would be a valuable tool compound to test the efficacy and safety associated with inhibiting group 1 PAK isoforms.

We have previously reported on an aminopyrazole scaffold-based series of PAK1 inhibitors that harness the ribose pocket in order to improve PAK1 affinity and obtain selectivity over Group II PAKs.[10] As part of this effort, indole **1** (Table 1) represented an attractive, non-basic scaffold with high PAK1 affinity (K_i = 31 nM). Compound **1** displayed activity in a phospho-S298-MEK1 (pMEK) EBC-1 cellular assay (IC_{50} = 120 nM) and was used as a tool molecule for mechanistic studies in the PAK1 pathway. Unfortunately, this compound was highly lipophilic ($c\log D = 4.4$)[11] and was not progressed due to the likelihood of ADME liabilities.[12] Our expectation was that the change from a phenyl to a pyridyl ring would, as a result of decreasing lipophilicity, improve drug-like properties, such as solubility and metabolic stability.[13] We further postulated

* Corresponding author. Tel.: +1 (650) 225 7704; fax: +1 (650) 742 4943.
E-mail address: wendyle@gene.com (W. Lee).
† Present address: Department of Biology, Blueprint Medicines, 215 First Street, Cambridge, MA 02142, USA.
‡ Present address: Novartis Institutes for BioMedical Research, 250 Massachusetts Avenue, Cambridge, MA 02139, USA.

http://dx.doi.org/10.1016/j.bmcl.2016.06.031
0960-894X/

Table 1
SAR of indole isosteres as PAK1 inhibitors

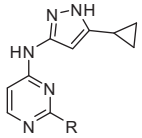

Compd	R	PAK1[a] K_i (nM)	PAK4/PAK1 selectivity	LLE[b]	*c*Log*D*[c]	Calcd pK_a[d] of indole NH	p-MEK[e] IC_{50} (nM)
1	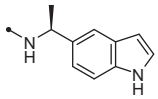	31	1.4	3.1	4.4	15.6	120
2	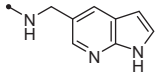	70	1.6	3.7	3.2	14.6	–
3	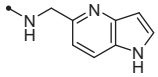	120	4.2	3.9	3.0	13.7	–
4	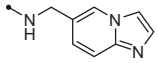	360	1.6	3.2	3.0	–	–
5	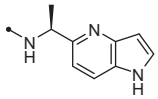	32	2.9	3.8	3.6	13.1	51
6	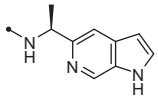	5	4.8	4.8	3.4	13.9	68

[a] PAK1 assay results represent the geometric mean of a minimum of two determinations performed in duplicate.
[b] Ligand-lipophilicity efficiency (LLE) was calculated using the equation: $-\log_{10}(\text{PAK } K_i) - c\log D\ (\text{pH}_{7.4})$.
[c] The *c*log*D* at pH7.4 was calculated using the Moka software (version 1.2.0, Molecular Discovery).
[d] Calculated using MoKa software (version 1.2.0, Molecular Discovery).
[e] p-MEK assay results represent the geometric mean of a minimum of two determinations.

that the additional nitrogen might improve PAK1 potency by reducing the pK_a of the donor NH of the indole, allowing for a stronger hydrogen-bonding interaction with the backbone carbonyl of Asp393 in the ribose pocket.[14]

We first prepared simple azaindoles **2** and **3** (Table 1). Although **3** was not as potent in our PAK1 biochemical assay, we were encouraged by the modest gain in ligand-lipophilicity efficiency (**3**: LLE = 3.9)[15] and the improved selectivity over PAK4 (**3**: 4.2-fold; PAK4 K_i = 505 nM) relative to **1**. The loss in biochemical potency with imidazopyridine **4** underscored the importance of the indole NH as a hydrogen donor moiety in PAK1. Given these factors and the favorable calculated pK_a value of the azaindole NH in **3** relative to **2**, we decided to incorporate the methyl group of **1** with the 4-azaindole analog. Azaindole **5** was found to be equipotent to **1** in PAK1, with a gain in ligand–lipophilicity efficiency (**5**: LLE = 3.8, **1**: LLE = 3.1) and a 2-fold increase in selectivity for PAK1 over PAK4 (**5**: PAK4/PAK1 = 2.9, **1**: PAK4/PAK1 = 1.4). Compound **5** also showed greater than two-fold improvement in pMEK (S298) cellular activity. 6-Azaindole **6** completed the nitrogen walk around the phenyl ring. Although **6** showed a 6-fold improvement in biochemical potency relative to **1**, the pMEK (S298) cellular activity for **6** was equipotent to **5** with a greater biochemical-to-cell shift (13.6-fold) relative to **5** (1.6-fold).

To enable further optimization of this 4-azaindole motif, we obtained a co-crystal structure of **5** in complex with PAK1 (Fig. 1). The pyrazole amine makes the expected donor–acceptor–donor hydrogen bond interactions with kinase hinge residues Glu345 and Leu347, in addition to a favorable hydrogen bond interaction measuring 2.8 Å from the azaindole NH to the backbone carbonyl of Asp393. The cyclopropyl moiety efficiently fills the space alongside the (Met) gatekeeper side chain. In the tail area, the methyl group α to the pyrrolopyridinyl amine fits well within the receptor surface and points toward the glycine-rich loop (P-loop) when in the (*S*)-configuration (Fig. 1B). In contrast, the (*R*)-enantiomer loses 21-fold PAK1 affinity (PAK1 IC_{50} = 685 nM). Modeling of this analog in the X-ray structure of **5** suggested the (*R*)-methyl moiety would clash with the aminopyrazole head group and adopt a more strained conformation.

Since **5** had a favorable physicochemical profile with a lower log*D* (*c*log*D*/log$D_{7.4}$ = 3.6/2.7) and good cellular potency, we next set out to evaluate the SAR around the 4-azaindole motif. Table 2 summarizes the SAR of aminopyrazole analogs with various substituted 4-azaindole tails (**7**–**10**). Modeling indicated that extending the (*S*)-α-methyl vector might be tolerated due to the large degree of flexibility in the glycine-rich loop in the PAK1 kinase domain.[17] Elongation to an ethyl group as in **7** resulted in retained PAK1 biochemical potency with a small improvement in selectivity over PAK4 (6.5-fold). Further exploration at this position was not pursued due to the decrease in LLE as a result of higher *c*log*D* (4.1) coupled with a 3-fold drop in cellular potency. We next investigated the SAR of 4-azaindole analogs that were substituted with halogens. The 6-fluoro-azaindole **8** had significantly improved PAK1 affinity (K_i = 4 nM) with similar potency to **5** in the cell-based assay. However, the corresponding 6-chloro analog **9** led to a 30-fold drop in biochemical potency (K_i = 119 nM) compared to **8**. This likely resulted from an altered conformational preference due to a steric clash between the chloro substituent and its adjacent amino methine linker. Interestingly, the 3-chloro azaindole **10** was equipotent to **8**, indicating that incorporation of a halogen on the pyrrole portion of the azaindole could also improve PAK1

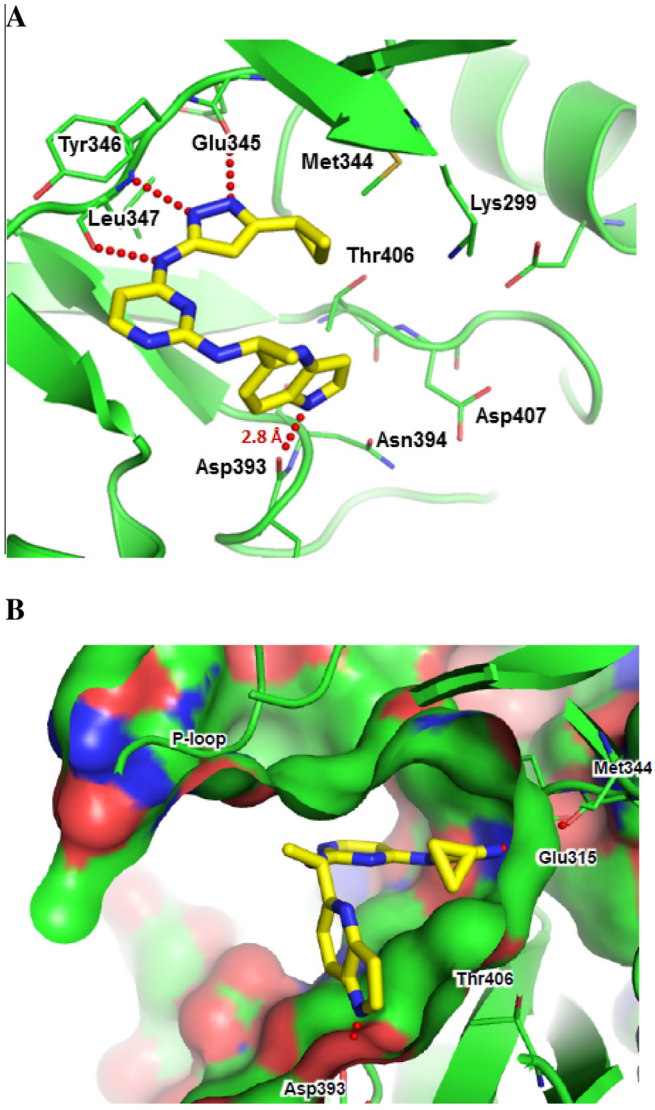

Figure 1. Co-crystal structure of inhibitor **5** (in yellow) in complex with PAK1 displayed from two different orientations.[16] (A) Hydrogen bond interactions are indicated with dotted red lines. The ligand forms hydrogen bond interactions with kinase hinge residues Glu345 and Leu347, and a crucial interaction between the azaindole NH to a backbone carbonyl of Asp393 in the ribose pocket. (B) Different orientation of inhibitor **5** shows the (*S*)-α-methyl moiety pointing towards the glycine-rich loop (P-loop).

potency. A possible explanation is that lowering the pK_a of the donor NH relative to **5** increased its H-bond donor strength.[14] Compound **10** also exhibited the best PAK1 over PAK4 selectivity (24-fold) for this sub-series. We attributed this selectivity to different spatial constraints in the ribose binding pockets of PAK1 and PAK4.[18] While Asn294 in PAK1 allows Asp407 to point away from the ligand, the corresponding PAK4 residue Ser445 in PAK4 orients the matching Asp group (Asp458) towards the ligand. Molecular modeling studies of **10** in PAK4 showed that the chloro substituent at the 3-azaindole position could clash with Asp458, possibly forcing the molecule to adopt a more strained conformation and preventing an optimal NH bond interaction with the backbone carbonyl group of Asp444.

We also combined the azaindole tail in **5** with different substituents around the aminopyrazole head group to determine whether potency and PAK1 selectivity could be further increased (Table 3). Previous SAR studies had demonstrated that small carbocycles, such as cyclopropyl or cyclobutyl, fit well in the deep front pocket alongside the (Met) gatekeeper.[10] Fluorine substitution is a commonly used measure to enhance biological activity and potentially increase metabolic stability of drug molecules.[19] We postulated that the incorporation of a mono-alkyl fluorine could further improve the physicochemical properties of our analogs by decreasing lipophilicity.[20] All four fluoro-substituted isomers at the 2-position of the cyclopropyl pyrazole head group were studied (**11**, **12**, **13**, and **14**). The *trans* (1*R*,2*S*)-fluoro cyclopropyl analog **11** showed superior PAK4 selectivity (11-fold) without any detriment to PAK1 biochemical potency (K_i = 11 nM) or cellular potency (IC_{50} = 77 nM). The *trans* (1*S*,2*R*)-fluoro cyclopropyl (**14**) diastereomer was also active in the PAK1 biochemical (K_i = 25 nM) and p-MEK cellular (IC_{50} = 92 nM) assays, but less selective against PAK4 (4.8-fold) relative to **11**. Other derivatives such as the *cis*-2-fluorocyclopropyls (**12**, **13**) and the difluorocyclobutyl analog **15** exhibited decreased PAK1 potencies and offered no advantages over **5**. We also masked the seemingly nonessential hydrogen at the secondary amino linker to the pyrimidine ring. While the *N*-methylated amino linked compound (**16**) had superior PAK1 potency (K_i = 18 nM) without compromising selectivity versus PAK4 (7-fold), it showed decreased cellular potency.

Prior to conducting in vivo mouse pharmacokinetics (PK) with the azaindole inhibitors, we profiled in vitro ADME properties for several selected examples. The molecules selected exhibited potent p-MEK(S298) cellular activity of less than 100 nM (Table 4). Based on in vitro metabolic stability, we were unable to differentiate between the indoles and azaindoles since all of the selected compounds were relatively labile in mouse liver microsomes (MLM) and moderate to labile in human liver microsomes (HLM). On the other hand, the 4-azaindoles (**5**, **8**, **11**, **14**) exhibited improved permeability (MDCK P_{app} A:B $\geqslant$ 3.7) over indole **1** (MDCK P_{app} A:B, 2.0) and 6-azaindole **6** (MDCK P_{app} A:B, 0.9). Mouse plasma protein binding for the azaindoles ranged from 95.3% to 98.6% bound (f_u = 0.047–0.014), representing a significant decrease over the unbound fraction of indole **1** (f_u = 0.008). Furthermore, with the exception of compound **8**, the azaindoles showed improved aqueous solubility (73–133 μM) relative to indole **1** (69 μM). Taken together, inhibitor **5** exhibited the best combination of cellular potency, MDCK permeability, plasma protein binding, and aqueous solubility and was progressed to in vivo mouse PK studies.

Table 5 shows the pharmacokinetic (PK) profile of indole **1** and 4-azaindole **5** in mice. Indole **1** exhibited clearance well above hepatic blood flow (mouse iv CL_p 160 mL/min/kg), which is under-predicted by in vitro liver microsome and hepatocyte stability data (MLM CL_{hep} = 76 mL/min/kg, MH CL_{hep} = 56 mL/min/kg), suggesting that extra-hepatic clearance mechanisms play a role. In contrast, the in vivo mouse clearance observed for **5** (mouse iv CL_p, 48 mL/min/kg) was comparable to that extrapolated from in vitro mouse hepatocyte clearance data (MH CL_{hep} = 52 mL/min/kg). When corrected for protein binding, the unbound mouse clearance in **5** (CL_u = 1067 mL/min/kg) is about 20-fold lower than **1** (CL_u = 20,000 mL/min/kg). Inhibitor **5** also showed measurable, albeit low, oral bioavailability (% *F* = 4.8).

To aid future compound design, we examined compounds **1** and **5** in additional DMPK assays. Our main intent was to identify the major routes of elimination and to understand the discrepancy between in vitro prediction and in vivo observation of **1**. For example, transporter-mediated hepatic uptake could be a rate-determining step in the hepatic clearance that could cause under-prediction of clearance extrapolated from in vitro metabolic stability assays.[21] In our studies, no active uptake was observed in mouse hepatocytes for **1** and **5**, indicating that hepatic transporters were not involved in the elimination process.[22] In a cytochrome P450 (CYP) assay using mouse liver microsomes (MLM) incubated with and without 1-aminobenzotriazole (ABT, an inactivator of cytochrome P450 enzymes used to discern CYP- from non

Table 2
Effect of substitutions around the azaindole motif

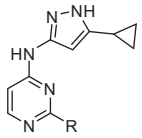

Compd	R	PAK1[a] K_i (nM)	PAK4/PAK1 selectivity	LLE[b]	*c*log*D*[c]	p-MEK[d] IC_{50} (nM)	Calc. pK_a[e] of indole NH
5	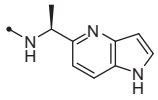	32	2.9	3.8	3.6	51	13.1
7	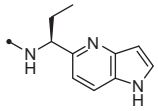	23	6.5	3.7	4.1	180	13.1
8	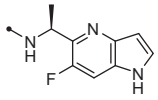	4	6	4.6	3.9	57	12.5
9	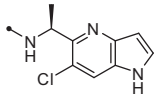	120	4	2.4	4.4	190	12.7
10	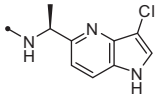	6	24	4.1	4.1	160	10.8

[a] PAK1 assay results represent the geometric mean of a minimum of two determinations performed in duplicate.
[b] Ligand-lipophilicity efficiency (LLE) was calculated using the equation: $-\log_{10}(\text{PAK } K_i) - c\log D\ (\text{pH}_{7.4})$.
[c] The *c*log*D* at pH7.4 was calculated using the Moka software (version 1.2.0, Molecular Discovery).
[d] p-MEK assay results represent the geometric mean of a minimum of two determinations.
[e] Calculated using MoKa software (version 1.2.0, Molecular Discovery).

Table 3
Structure–activity relationships of 4-azaindoles

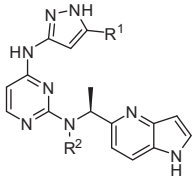

Compd	R^1	R^2	PAK1[a] K_i (nM)	PAK4/PAK1 selectivity	LLE[b]	*c*Log*D*[c]	p-MEK[d] IC_{50} (nM)
5		H	32	2.9	3.8	3.6	51
11		H	11	11.4	3.6	3.4	77
12		H	120	2.8	3.5	3.4	810
13		H	84	5.7	3.7	3.4	270
14		H	25	4.8	4.2	3.4	92
15		H	68	6.6	3.1	4.1	250
16		Me	18	7	3.6	4.1	240

[a] PAK1 assay results represent the geometric mean of a minimum of two determinations performed in duplicate.
[b] Ligand-lipophilicity efficiency (LLE) was calculated using the equation: $-\log_{10}(\text{PAK } K_i) - c\log D\ (\text{pH } 7.4)$.
[c] The *c*log*D* at pH7.4 was calculated using the Moka software (version 1.2.0, Molecular Discovery).
[d] p-MEK assay results represent the geometric mean of a minimum of two determinations.

Table 4
In vitro ADME properties of indole **1** and selected azaindole PAK1 inhibitors

Compd	pMEK (S298) IC_{50}[a] (nM)	MLM[b]/HLM[c] CL_{hep} (mL/min/kg)	MDCK P_{app} A:B (10^{-6} cm/s)[d]	Mouse PPB (f_u)[e]	Solubility[f] (μM)
1	120	76/13	2.0	0.008	69
5	51	76/13	4.3	0.045	133
6	68	77/11	0.9	0.039	73
8	57	76/12	8.3	0.014	58
11	72	78/15	3.7	–	104
14	92	78/15	4.2	0.047	73

[a] p-MEK assay results represent the geometric mean of a minimum of two determinations.
[b] Mouse hepatic clearance predicted from mouse liver microsomes intrinsic CL.
[c] Human hepatic clearance predicted from human liver microsomes intrinsic CL.
[d] Permeability in Madin–Darby Canine Kidney (MDCK) cells, apical-to-basolateral flux.
[e] Mouse plasma protein binding expressed as fraction unbound.
[f] Kinetic aqueous solubility at pH 7.4 as determined from a single experiment in a high-throughput solubility assay.

Table 5
Comparison of in vivo PK properties of indole **1** and azaindole **5** in nude mice.[a]

Route	Compd	Dose[a] (mg/kg)	C_{max}[b] (μM)	T_{max}[c] (h)	V_{ss} (L/kg)[d]	CL_p/CL_u[e] (mL/min/kg)	$t_{1/2}$[f] (h)	% F[g]	MH[h]
iv	**1**	2	–	–	4.50	160/20,000	0.32	–	56
iv	**5**	2	–	–	1.65	48/1067	0.63	–	52
po	**5**	25	4.7	0.58	–	–	–	4.8	–

[a] Formulations used: iv 40:60 PEG400/H_2O (solution); po 60:40 PEG400/H_2O.
[b] Maximum plasma concentration.
[c] Time at which maximum plasma concentration was observed.
[d] Volume of distribution at steady-state.
[e] Clearance unbound = CL_p/f_u.
[f] Half-life.
[g] Oral bioavailibility.
[h] Mouse hepatic clearance predicted from *in vitro* mouse hepatocytes data.

Table 6
Additional in vitro ADME profiling of compounds **1** and **5**

CYP-mediated MLM ± ABT[a]		
	% **1** remaining after 30 min[b]	% **5** remaining after 30 min[b]
MLM − NADPH	81 ± 13	98 ± 8.5
MLM + NADPH	14 ± 0.94	10 ± 2.8
MLM + ABT	59 ± 5.9	94 ± 13
MDCK-MDR1[c]		
	1	**5**
P_{app} A:B (10^{-06} cm/s)	0.5	0.2
P_{app} B:A (10^{-06} cm/s)	14.6	9.8
Efflux ratio	27.7	59

[a] CYP-mediated mouse liver microsomes ± ABT (1-aminobenzotriazole). Compounds were preincubated with NADPH for 20 min before addition of 1 mM of ABT.
[b] Determined by $n = 3$.
[c] Human P-glycoprotein (P-gp) transfected in Madin Darby canine kidney (MDCK-MDR1) cell permeability assay.

CYP-mediated metabolism), we observed a significant reduction in disappearance of the parent compounds after 30 min incubation in the presence of ABT, suggesting that P450-mediated metabolism was responsible for the in vitro mouse clearance observed for **1** and **5** (Table 6). In a permeability assay with human P-glycoprotein (P-gp) transfected in Madin Darby canine kidney (MDCK-MDR1) cells (Table 6), both **1** and **5** exhibited low permeability (P_{app} A:B **1**: 0.5×10^{-6} cm/s; **5**: 0.2×10^{-6} cm/s) with high efflux ratios (B:A/A:B, **1**: 27.7; **5**: 59), indicating that these compounds are P-gp substrates. It is known that for compound with low permeability, P-gp efflux could play a role in limiting the absorption of compounds by driving the drug back into the lumen.[23] Thus, it was likely a combination of the factors outlined above, moderate first-pass clearance, moderate passive permeability, and P-gp-mediated efflux that resulted in the low oral bioavailability of **5**.

The preparation of the diaminopyrimidines **5** and **6** is depicted in Scheme 1; this general route was used for the synthesis of diaminopyrimidines **1**–**16**. Commercially available cyclopropyl-1*H*-pyrazol-5-amine **17** was reacted with 2,4-dichloropyrimidine via an S_NAr reaction to yield the corresponding monofunctionalized pyrimidine **18**. Additional mono-substituted pyrimidine intermediates were prepared via this method using mono-fluoro-cyclopropyl-1*H*-pyrazol-5-amines[24] or commercially available (3,3-difluorocyclobutyl)-1*H*-pyrazol-5-amine. A second S_NAr reaction on **18** with bicyclic amines such as **19** afforded the desired diaminopyrimidine **5**. Compounds **1**–**4** were prepared from commercially available bicyclic amines. In cases where the azaindoles were *N*-protected, acid or base mediated deprotection was required as a final step. For racemic amines such as **20**,[25] a chiral separation was required to give the desired (*S*)-α-methyl stereoisomer, as with **6**.

For the synthesis of **19**, we employed a stereospecific approach to install the (*S*)-α-methyl group using Ellman's chiral auxiliary as shown in Scheme 2.[26] Stille coupling of tri-*n*-butyl-1-ethoxyvinyl-stannane with Boc-protected 5-chloro-1*H*-pyrrolo[3,2-*b*]pyridine **22** provided the 1-ethoxyvinyl derivative, which could be readily hydrolyzed to the corresponding ketone **23a**. The *N*-Boc-protected ketone **25a** was then condensed with (*R*)-2-methylpropane-2-sulfinamide. Reduction of the sulfinamide and acid-mediated removal of the chiral functionality afforded the desired (*S*)-1-(1*H*-pyrrolo[3,2-*b*]pyridin-5-yl)ethan-1-amine, **28a**, as the HCl salt. Using this method, the 3-chloro derivative **28b** and the one-carbon elongated, (*S*)-α-ethyl, analog **28c** were prepared from **25b** and **25c**, respectively. Intermediate **25b** was synthesized via chlorination of **23a** with *N*-chlorosuccinimide followed by Boc protection. A direct palladium-catalyzed cyanation of **22** afforded **24**. Grignard reaction on **24** using ethyl magnesium bromide afforded intermediate **25c**

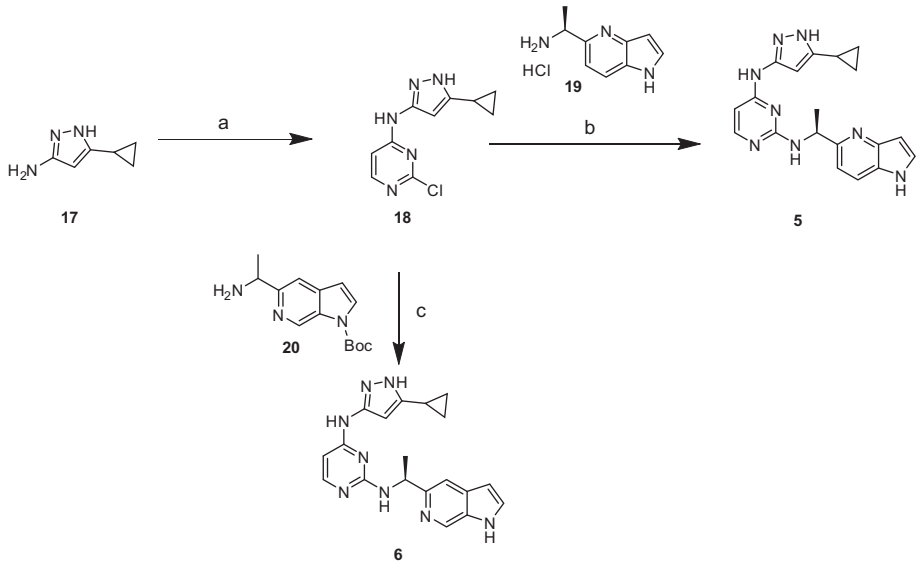

Scheme 1. Preparation of diaminopyrimidines. Reagents and conditions: (a) 2,4-dichloropyrimidine, DMA, Et_3N, 120 °C, 16 h; (b) **19**, DIPEA, ^{n}BuOH, 115 °C, sealed tube, 18 h, 84% yield (2-steps); (c) (i) **20**, DIPEA, ^{n}BuOH, 115 °C, sealed tube, 18 h; (ii) 4 N HCl in dioxane, MeOH, 40 °C, chiral separation, 19% yield (2-steps).

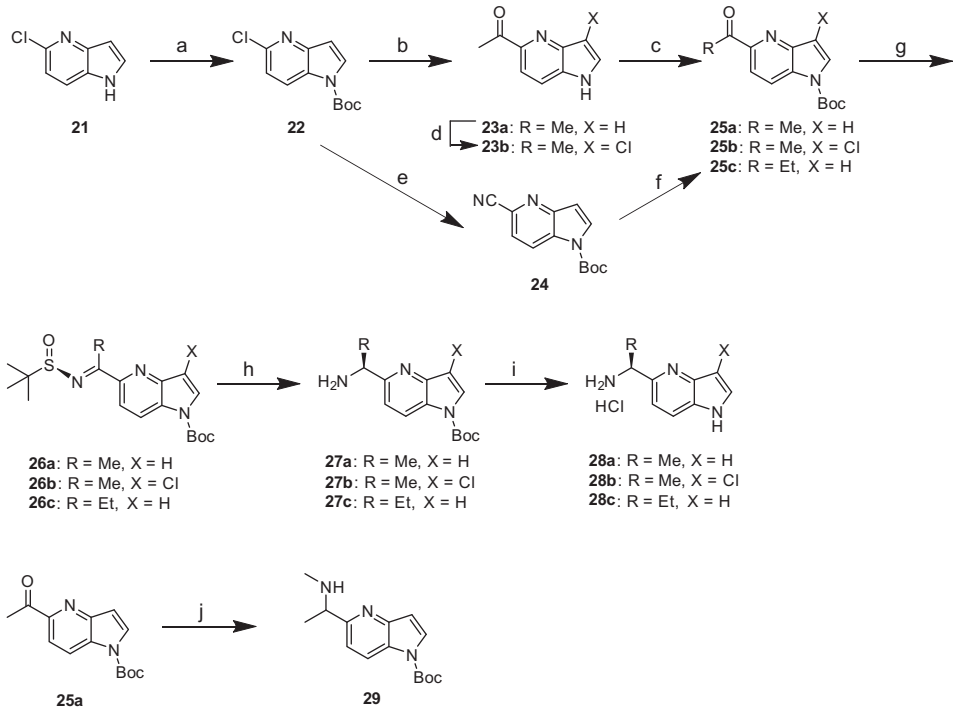

Scheme 2. Enantioselective synthesis of **28** and analogs thereof. Reagents and conditions: (a) di-*tert*-butyl dicarbonate, DMAP, ACN, 0 °C to rt, 99%; (b) (i) tributyl(1-ethoxyvinyl)stannane, $Pd(PPh_3)_4$, DMF, 100 °C, sealed tube; (ii) 2 N HCl, THF, rt, 64%; (c) di-*tert*-butyl dicarbonate, DMAP, ACN, 0 °C to rt, 82–88%; (d) *N*-chlorosuccinimide, DMF, 0 °C to rt, 96%; (e) zinc cyanide, zinc powder, $Pd_2(dba)_3$, 1,1′-bis(diphenylphosphino)ferrocene, *N*-methylmorpholine, 180 °C, 75%; (f) ethyl magnesium bromide (2 M in THF), THF, −20 to 10 °C, 64%; (g) (*R*)-2-methylpropane-2-sulfinamide, Ti(IV)(OEt)4, THF, 75 °C, 33–54%; (h) L-Selectride® (1 M in THF), THF, 0 °C to rt, 73–81%; (i) 4 N HCl in dioxane, MeOH, 40 °C, 99%; (j) methylamine hydrochloride, sodium cyanoborohydride, EtOH, 130 °C, microwave, 94%.

following aqueous workup. A final S_NAr reaction, as depicted in Scheme 1, using **18** with **28b** or **28c** afforded the diaminopyrimidines **10** or **7**, respectively. For compound **16**, the *N*-methylated azaindole precursor **29** was prepared via a reductive amination of methyl ketone **25a** with methylamine.

The synthesis of 6-substituted fluoro- and chloro-azaindoles is outlined in Scheme 3. The indolyl nitrogen of **30a** and **30b** was protected with a tosyl group, followed by a modified Reissert-Henze reaction[27] to give the cyano products **33a** and **33b**. A Grignard reaction on **33a** and **33b** afforded methyl ketones **34a** and **34b**. Installation of the α-methyl amino group was accomplished by condensation of the ketones with hydroxylamine to form oximes and subsequent reduction to the primary amines gave the requisite intermediates **35a** and **35b**. Completion of the

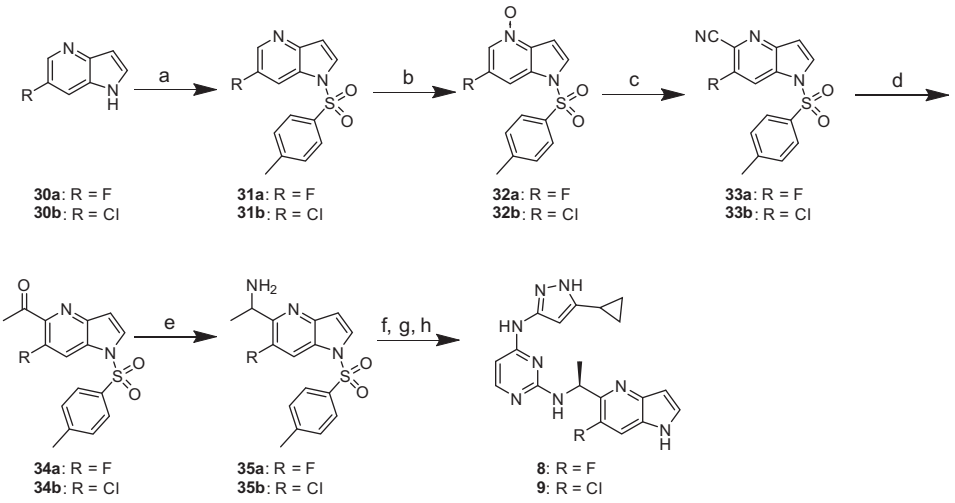

Scheme 3. Preparation of 6-halogenated-4-azaindoles. Reagents and conditions: (a) (i) sodium hydride, THF, 0 °C, 30 min; (ii) *p*-toluenesulfonyl chloride, 0 °C to rt, 18 h, 84–89%; (b) *m*CPBA, DCM, 0 °C to rt, 2 h, 90–95%; (c) dimethylcarbamyl chloride, trimethylsilyl cyanide, DCE, 80 °C, 20 h, 53–56%; (d) methyl magnesium chloride (1 M in THF), THF, −10 to 0 °C, 1.5 h, 18–20%; (e) (i) hydroxylamine hydrochloride, sodium acetate, EtOH, rt, 18 h; (ii) zinc powder, ammonium chloride, AcOH, MeOH, reflux, 20 h, 78–81% (2-steps); (f) **18**, 2,4-dimethyl-3-pentanol, DIPEA, 140 °C, 18 h; (g) chiral SFC separation; (h) KOH (2 N), MeOH, 100 °C, 3 h, 26–30%.

syntheses following the established route of base-mediated S_NAr reaction, chiral separation, and protecting group removal gave the desired 6-halogenated azaindoles **8** and **9**, respectively.

In summary, we were able to improve the physicochemical properties through lowering lipophilicity of our aminopyrazole scaffold-based PAK1 inhibitor **1** by replacing the indole moiety with a 4-azaindole motif. A stereospecific approach to the installation of the (*S*)-α-methyl group of the azaindole tail was developed that utilized Ellman's chiral auxiliary. This resulted in the identification of **5**, representing a 2-fold improvement in cellular potency and a slight enhancement in selectivity against PAK4. Modulation of the pK_a of the aza-indolic NH by incorporating a halogen led to additional analogs with superior PAK1 biochemical activity (K_i <10 nM) and increased selectivity versus PAK4 (up to 24-fold). As expected, the decrease in lipophilicity of azaindole **5** (log*D* = 2.7) contributed to improved aqueous solubility and lower plasma protein binding than indole **1** (log*D* = 3.7). In mouse PK studies, azaindole **5** displayed moderate in vivo clearance (48 mL/kg/min) and low oral bioavailability (% *F* = 4.8). When corrected for protein binding, the unbound mouse clearance for **5** (CL_u = 1067 mL/min/kg) was nearly 20-fold lower than **1** (CL_u = 20,000 mL/min/kg).

Acknowledgement

We thank the purification and analytical groups within Genentech Small Molecule Drug Discovery for their support.

Supplementary data

Supplementary data associated with this article can be found, in the online version, at http://dx.doi.org/10.1016/j.bmcl.2016.06.031.

References and notes

1. Radu, M.; Semenova, G.; Kosoff, R.; Chernoff, J. *Nat. Rev. Cancer* **2014**, *14*, 13.
2. Baskaran, Y.; Ng, Y. W.; Selamat, W.; Ling, F. T. Y.; Manser, E. *EMBO Rep.* **2012**, *13*, 653.
3. Ha, B. H.; Morse, E. M.; Turk, B. E.; Boggon, T. J. *J. Biol. Chem.* **2015**, *290*, 12975.
4. King, H.; Nicholas, N. S.; Wells, C. M. *Int. Rev. Cell Mol. Biol.* **2014**, *309*, 347.
5. (a) Huynh, N.; Liu, K. H.; Baldwin, G. S., et al. *Biochim. Biophys. Acta* **2010**, *1803*, 1106; (b) Ong, C. C.; Jubb, A. M.; Haverty, P. M.; Zhou, W.; Tran, V.; Truong, T.; Turley, H.; O'Brien, T.; Vucic, D.; Harris, A. L.; Belvin, M.; Friedman, L. S.; Blackwood, E. M.; Koeppen, H.; Hoeflich, K. P. *Proc. Natl. Acad. Sci. U.S.A.* **2011**, *108*, 7177; (c) Ong, C. C.; Jubb, A. M.; Jakubiak, D.; Zhou, W.; Rudolph, J.; Haverty, P. M.; Kowanetz, M.; Yan, Y.; Tremayne, J.; Lisle, R.; Harris, A. L.; Friedman, L. S.; Belvin, M.; Middleton, M. R.; Blackwood, E. M.; Koeppen, H.; Hoeflich, K. P. *J. Natl. Cancer Inst.* **2013**, *105*, 606.
6. (a) Crawford, J. J.; Hoeflich, K. P.; Rudolph, J. *Expert Opin. Ther. Pat.* **2012**, *22*, 293; (b) Rudolph, J.; Crawford, J. J.; Hoeflich, K. P.; Chernoff, J. *Enzymes* **2013**, *34*, 157; (c) Rudolph, J.; Crawford, J. J.; Hoeflich, K. P.; Wang, W. *J. Med. Chem.* **2015**, *58*, 111; (d) Xu, Y.; Foulks, J. M.; Clifford, A.; Brenning, B.; Lai, S.; Luo, B.; Parnell, K. M.; Merx, S.; McCullar, M. V.; Kanner, S. B.; Ho, K. *Bioorg. Med. Chem. Lett.* **2013**, *23*, 4072.
7. Ndubaku, C. O.; Crawford, J. J.; Drobnick, J.; Aliagas, I.; Campbell, D.; Dong, P.; Dornan, L. M.; Duron, S.; Epler, J.; Gazzard, L.; Heise, C. E.; Hoeflich, K. P.; Jakubiak, D.; La, H.; Lee, W.; Lin, B.; Lyssikatos, J. P.; Maksimoska, J.; Marmorstein, R.; Murray, L. J.; O'Brien, T.; Oh, A.; Ramaswamy, S.; Wang, W.; Zhao, X.; Zhong, Y.; Blackwood, E.; Rudolph, J. *ACS Med. Chem. Lett.* **2015**, *6*, 1241.
8. Ong, C. C.; Gierke, S.; Pitt, C.; Sagolla, M.; Cheng, C. K.; Zhou, W.; Jubb, A. M.; Strickland, L.; Schmidt, M.; Duron, S. G.; Campbell, D. A.; Zheng, W.; Dehdashti, S.; Shen, M.; Yang, N.; Behnke, M. L.; Huang, W.; McKew, J. C.; Chernoff, J.; Forrest, W. F.; Haverty, P. M.; Chin, S.-F.; Rakha, E. A.; Green, A. R.; Ellis, I. O.; Caldas, C.; O'Brien, T.; Friedman, L. S.; Koeppen, H.; Rudolph, J.; Hoeflich, K. P. *Breast Cancer Res.* **2015**, *17*, 1.
9. Prudnikova, T. Y.; Villamar-Cruz, O.; Rawat, S. J.; Cai, K. Q.; Chernoff, J. *Oncogene* **2015**, *1*, 1.
10. Crawford, J. J.; Lee, W.; Aliagas, I.; Mathieu, S.; Hoeflich, K. P.; Zhou, W.; Wang, W.; Rouge, L.; Murray, L.; La, H.; Liu, N.; Fan, P. W.; Cheong, J.; Heise, C. E.; Sreemathy, R.; Mintzer, R.; Liu, Y.; Chao, Q.; Rudolph, J. *J. Med. Chem.* **2015**, *58*, 5121.
11. The measured log*D* for indole **1** is 3.7. We found that our calculated log*D* was over-estimated by 0.5–1.0 log unit. For design, we used *c*log*D* to compare the compounds in a relative rather than absolute sense.
12. Arnott, J. A.; Planey, S. L. *Expert Opin. Drug Discov.* **2012**, *7*, 863.
13. Blaazer, A. B.; Lange, J. H. M.; Van der Neut, M. A. W.; Mulder, A.; Den Boon, F. S.; Werkman, T. R.; Kruse, C. G.; Wadman, W. J. *Eur. J. Med. Chem.* **2011**, *46*, 5086.
14. Gilli, P.; Pretto, L.; Bertolasi, V.; Gilli, G. *Acc. Chem. Res.* **2009**, *42*, 33.
15. Leeson, P. D.; Springthorpe, B. *Nat. Rev. Drug Disc.* **2007**, *6*, 881.
16. See Supplementary material for experimental detail describing PAK1 crystal experiment.
17. (a) Lei, M.; Lu, W.; Meng, W.; Parrini, M.; Eck, M. J.; Mayer, B. J.; Harrison, S. C. *Cell* **2000**, *102*, 387; (b) Meggers, E. *Angew. Chem., Int. Ed.* **2011**, *50*, 2442.
18. See Ref. 10 for an explanation of the PAK1 versus PAK4 enzymes and comparison of crystal structures of a PAK1 inhibitor in PAK1 versus PAK4 enzyme.
19. (a) Purser, S.; Moore, P. R.; Swallow, S.; Gouverneur, V. *Chem. Soc. Rev.* **2008**, *37*, 320; (b) Shah, P.; Westwell, A. D. *J. Enzyme Inhib. Med. Chem.* **2007**, *22*, 527.
20. (a) Gillis, E. P.; Eastman, K. J.; Hill, M. D.; Donnelly, D. J.; Meanwell, N. A. *J. Med. Chem.* **2015**, *58*, 8315; (b) Smart, B. E. *J. Fluorine Chem.* **2001**, *109*, 3.
21. Chiba, M.; Ishii, Y.; Sugiyama, Y. *AAPS J.* **2009**, *11*, 262.
22. See Supplementary material for data.
23. Chan, K. M. S.; Lowes, S.; Hirst, B. H. *Eur. J. Pharm. Sci.* **2004**, *21*, 25.
24. See Supplementary material for scheme describing the preparation of mono-fluoro-cyclopropyl-1*H*-pyrazol-5-amines.
25. See Supplementary material for scheme describing the synthesis of *tert*-butyl 5-(1-aminoethyl)-1*H*-pyrrolo[3,2-*b*]pyridine-1-carboxylate **20**.
26. Tanuwidjaja, J.; Peltier, H. M.; Ellman, J. *J. Org. Chem.* **2007**, *72*, 626.
27. Fife, W. K. *J. Org. Chem.* **1983**, *48*, 1375.